Author Manuscript

Author Manuscript

Author Manuscript

Author Manuscript

HHS Public Access

Author manuscript

Cell Rep. Author manuscript; available in PMC 2022 May 12.

Published in final edited form as:

Cell Rep. 2022 April 19; 39(3): 110716. doi:10.1016/j.celrep.2022.110716.

Inhibitory co-transmission from midbrain dopamine neurons relies on presynaptic GABA uptake

Riccardo Melani[1,2], **Nicolas X. Tritsch**[1,2,3,*]

[1]Neuroscience Institute, New York University Grossman School of Medicine, New York, NY 10016, USA

[2]Fresco Institute for Parkinson's and Movement Disorders, New York University Langone Health, New York, NY 10016, USA

[3]Lead contact

SUMMARY

Dopamine (DA)-releasing neurons in the substantia nigra pars compacta (SNc^{DA}) inhibit target cells in the striatum through postsynaptic activation of γ-aminobutyric acid (GABA) receptors. However, the molecular mechanisms responsible for GABAergic signaling remain unclear, as SNc^{DA} neurons lack enzymes typically required to produce GABA or package it into synaptic vesicles. Here, we show that aldehyde dehydrogenase 1a1 (Aldh1a1), an enzyme proposed to function as a GABA synthetic enzyme in SNc^{DA} neurons, does not produce GABA for synaptic transmission. Instead, we demonstrate that SNc^{DA} axons obtain GABA exclusively through presynaptic uptake using the membrane GABA transporter Gat1 (encoded by *Slc6a1*). GABA is then packaged for vesicular release using the vesicular monoamine transporter Vmat2. Our data therefore show that presynaptic transmitter recycling can substitute for de novo GABA synthesis and that Vmat2 contributes to vesicular GABA transport, expanding the range of molecular mechanisms available to neurons to support inhibitory synaptic communication.

In brief

Melani and Tritsch demonstrate that inhibitory co-transmission from midbrain dopaminergic neurons does not depend on cell-autonomous GABA synthesis but instead on presynaptic import from the extracellular space through the membrane transporter Gat1 and that GABA loading into synaptic vesicles relies on the vesicular monoamine transporter Vmat2.

This is an open access article under the CC BY-NC-ND license (http://creativecommons.org/licenses/by-nc-nd/4.0/).

*Correspondence: nicolas.tritsch@nyulangone.org.

AUTHOR CONTRIBUTIONS

R.M. and N.X.T. designed and performed experiments, analyzed and interpreted the data, and wrote the manuscript.

DECLARATION OF INTERESTS

The authors declare no competing interests.

INCLUSION AND DIVERSITY

We worked to ensure sex balance in the selection of non-human subjects. The author list of this paper includes contributors from the location where the research was conducted who participated in the data collection, design, analysis, and/or interpretation of the work.

SUPPLEMENTAL INFORMATION

Supplemental information can be found online at https://doi.org/10.1016/j.celrep.2022.110716.

Author Manuscript Author Manuscript Author Manuscript Author Manuscript

Graphical Abstract

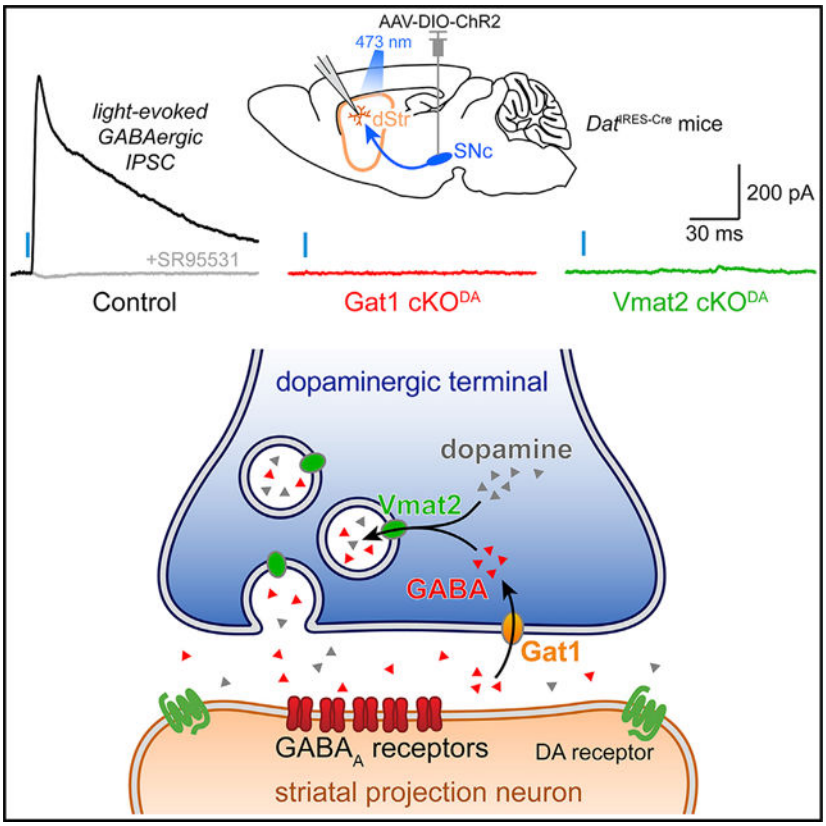

INTRODUCTION

A detailed appreciation for how neurons modify the activity of surrounding cells through the release of transmitters is key to our understanding of the brain. Because neurons rely primarily on the release of a single classical neurotransmitter to transmit signals across synapses, it is typically sufficient to manipulate the activity of presynaptic cells to evaluate their postsynaptic contribution. However, this approach is insufficient for neurons that release multiple classical transmitters. Chief among them are midbrain neurons of the substantia nigra pars compacta (SNc). These cells are best known for their ability to release dopamine (DA), but they can also directly affect the discharge of target cells in striatum through monosynaptic glutamatergic and GABAergic signaling (Hnasko et al., 2010; Tecuapetla et al., 2010; Tritsch et al., 2012; Trudeau et al., 2014). The molecular mechanisms that enable glutamate co-release from DA-releasing SNc (SNc^{DA}) neurons are well established (Eskenazi et al., 2021). By contrast, much less is known about inhibitory co-transmission (Tritsch et al., 2016).

An important contributor to this gap in knowledge is that nigrostriatal DAergic neurons do not possess the molecular machinery thought to be essential for GABAergic synaptic transmission; they do not express the GABA synthetic enzymes Gad65 and Gad67 or the vesicular GABA transporter Vgat (Poulin et al., 2014; Saunders et al., 2018; Tritsch et al.,

Author Manuscript Author Manuscript Author Manuscript Author Manuscript

2012, 2014). Instead, inhibitory co-transmission from SNc^{DA} neurons was proposed to rely on the vesicular monoamine transporter Vmat2 (Tritsch et al., 2012), which is not known to transport GABA (Yelin and Schuldiner, 1995). Several endogenous ligands activate $GABA_A$ receptors (R) (Belelli and Lambert, 2005; Johnston, 1996); it is therefore conceivable that the transmitter released by SNc^{DA} neurons is not GABA but a ligand that functions as a $GABA_AR$ agonist and serves as a substrate for Vmat2. Another possibility is that GABA is the transmitter but that the mechanisms involved remain to be defined. Both scenarios point to an incomplete understanding of molecular pathways that neurons can leverage to inhibit postsynaptic targets.

We previously suggested that SNc^{DA} neurons import GABA from the extracellular milieu, as they contain mRNA for the membrane GABA transporter Gat1 and pharmacological inhibition of GABA uptake impairs GABAergic co-transmission (Tritsch et al., 2014). However, a recent study found that Gat1 does not distribute to the axon of SNc^{DA} neurons and that Gat1 inhibition non-selectively depresses vesicular release from SNc^{DA} axons (Roberts et al., 2020). In addition, SNc^{DA} neurons were proposed to synthetize GABA *de novo* using the mitochondrial enzyme Aldh1a1 (Kim et al., 2015), which a subpopulation of SNc^{DA} neurons expresses abundantly (Liu et al., 2014; McCaffery and Dräger, 1994; Poulin et al., 2014). Here, we show that SNc^{DA} neurons do not produce GABA using Aldh1a1 but rely instead on Gat1-mediated uptake to obtain GABA for Vmat2-dependent vesicular release. Our data therefore demonstrate that membrane GABA transporters and vesicular monoamine transporters can respectively substitute for Gad-dependent GABA synthesis and Vgat-mediated vesicular loading, expanding the range of molecular mechanisms available to neurons to support inhibitory transmission.

RESULTS

Aldh1a1 does not directly contribute to inhibitory co-transmission from SNc^{DA} neurons

To examine how Adlh1a1 contributes to inhibitory transmission from SNc^{DA} neurons, we obtained Aldh1a1 germline knockout mice (*Aldh1a1*$^{-/-}$; Fan et al., 2003). Using immunofluorescence, we confirmed that Aldh1a1 is no longer detected in the brain of knockouts, including in SNc^{DA} neurons (Figures 1A and 1B). We next bred *Aldh1a1*$^{-/-}$ mice to *Dat*$^{IRES\text{-}Cre}$ knockin mice (Bäckman et al., 2006) to enable adeno-associated virus (AAV)-mediated expression of channelrhodopsin 2 (ChR2) in SNc^{DA} neurons (Figures S1A and S1B). We obtained acute brain slices from these mice, stimulated SNc^{DA} axons using 1-ms blue light flashes, and recorded $GABA_AR$ inhibitory postsynaptic currents (IPSCs) from striatal projection neurons (SPNs) using whole-cell voltage clamp (Figure 1C). We limited recordings to dorsal striatum where $Aldh1a1^+$ SNc^{DA} axons project most densely (Figures S2A and S2B). The amplitude of optogenetically evoked IPSCs (oIPSCs) in *Aldh1a1*$^{-/-}$ mice was reduced compared with controls, but not statistically different (Figure 1D). The synaptic latency (Figure 1D) and rise time of oIPSCs (Figure 1D), as well as their sensitivity to the $GABA_AR$ antagonist SR95531 (Figure S1C), were also comparable across conditions, indicating that genetic deletion of Aldh1a1 does not strongly impair the ability of SNc^{DA} neurons to inhibit SPNs.

Author Manuscript Author Manuscript Author Manuscript Author Manuscript

Because Aldh1a1 expression is not exclusive to SNc (Figures 1A and S2A), it is unclear whether the reduction in inhibitory co-transmission in *Aldh1a1*$^{-/-}$ mice results from the specific loss of Aldh1a1 in SNc^{DA} neurons. If Aldh1a1 functions as a GABA synthetic enzyme, we reasoned that selectively restoring its expression in SNc^{DA} neurons ought to increase inhibitory co-transmission in *Aldh1a1*$^{-/-}$ mice. We therefore generated an AAV expressing Cre-dependent Aldh1a1, which we co-injected along with Cre-dependent ChR2 in the midbrain of *Dat*$^{IRES\text{-}Cre/+}$;*Aldh1a1*$^{-/-}$ mice (Figures 1B and S1A). This manipulation reestablished Aldh1a1 protein expression in DA neurons (Figure 1B) but failed to increase the amplitude of oIPSCs in SPNs (Figure 1D).

To assess whether differences in ChR2 expression hindered our ability to reveal a role for Aldh1a1, we recorded optogenetically evoked excitatory postsynaptic currents (oEPSCs) from the same SPNs. oEPSCs reflect glutamate co-release (Trudeau et al., 2014) and therefore serve as an independent metric of stimulation strength. We did not observe differences in the prevalence, amplitude, and kinetics of oEPSCs across conditions (Figures 1E and S1D), indicating that we recruited similar numbers of SNc^{DA} axons. We nevertheless carried out an additional experiment to minimize variability in ChR2 expression: we expressed it genetically in all DAergic neurons by breeding a conditional allele of ChR2 (Madisen et al., 2012) into *Dat*$^{IRES\text{-}Cre/+}$;*Aldh1a1*$^{-/-}$ mice. Here, too, we failed to detect any difference in the amplitude of oIPSCs or oEPSCs in *Aldh1a1*$^{+/+}$ and *Aldh1a1*$^{-/-}$ mice (Figures S1E–S1G and S2C). Collectively, these results fail to support an important, cell-autonomous role for Aldh1a1 in producing GABA for inhibitory co-transmission from SNc^{DA} axons.

Selective deletion of Gat1 from SNc^{DA} neurons abolishes GABAergic co-transmission

SNc^{DA} neurons in mice do not express the canonical GABA synthetic enzymes Gad65 and Gad67 (Poulin et al., 2014; Tritsch et al., 2014; Saunders et al., 2018). If Aldh1a1 does not produce GABA either, how do SNc^{DA} neurons inhibit SPNs? We previously proposed that SNc^{DA} neurons acquire GABA using Gat1 (Tritsch et al., 2014). To test this directly, we generated mice in which Gat1 can be conditionally knocked out (cKO) by Cre recombinase (*Gat1*^{fl} mice; Figures 2A and S3A–S3D). To validate our strategy, we first deleted Gat1 constitutively by breeding *Gat1*^{fl} mice to a line expressing germline Cre (Gat1 cKO^{germline}). As shown in Figure 2B, Gat1 protein is not detected in the brain of Gat1 cKO^{germline} mice, confirming our ability to ablate Gat1 in a Cre-dependent fashion.

We next crossed *Gat1*^{fl} and *Dat*$^{IRES\text{-}Cre}$ mice to generate offspring in which Gat1 is selectively deleted from DAergic cells (*Dat*$^{IRES\text{-}Cre/+}$;*Gat1*$^{fl/fl}$ or Gat1 cKO^{DA} mice; Figures 2A, 2C, and S3A). Using *in situ* hybridization, we confirmed that Gat1 mRNA is no longer detected in SNc^{DA} neurons of Gat1 cKO^{DA} mice yet is intact in surrounding inhibitory neurons within the substantia nigra (Figures 2C, S3E, and S3F). To assess inhibitory co-transmission, we virally expressed ChR2 in SNc^{DA} neurons and recorded light-evoked postsynaptic currents in SPNs. Although oIPSCs are readily observed in control slices, they were entirely absent in Gat1 cKO^{DA} mice (Figures 2D–2E and S3G). Importantly, the same SPNs showed oEPSCs that were similar to controls in prevalence, amplitude, and kinetics (Figures 2D, 2F, and S3H), confirming our ability to stimulate SNc^{DA} neurons.

Author Manuscript Author Manuscript Author Manuscript Author Manuscript

Moreover, in mice in which Gat1 is conditionally knocked down in DAergic neurons (*Dat*$^{IRES\text{-}Cre/+}$;*Gat1*$^{fl/+}$ or Gat1 cKD^{DA} mice), oIPSCs were 60% smaller than controls but were otherwise comparable in prevalence and kinetics (Figures 2D, 2E, and S3G). These data suggest that Gat1 expression in SNc^{DA} neurons modulates the strength of inhibitory co-transmission onto SPNs in a dose-dependent fashion, with complete removal of Gat1 abolishing GABAergic signaling entirely.

Deleting Gat1 from SNc^{DA} neurons does not impair basic nigrostriatal physiology

Our inability to evoke oIPSCs in Gat1 cKO^{DA} mice may reflect deleterious effects of our manipulation on nigrostriatal function. To test this, we first determined whether Gat1 loss affects the development of SNc^{DA} neurons using immunofluorescence for the DA synthetic enzyme tyrosine hydroxylase (TH). Figures S4A–S4C show that the number of TH^{+} cell bodies in SNc and the density of TH^{+} axons in striatum are indistinguishable in control and Gat1 cKO^{DA} mice. We also did not observe any difference in TH or Aldh1a1 levels or in the cellular distribution of Aldh1a1 in SNc^{DA} neurons (Figures S4D and S4E), indicating that deleting Gat1 from DA neurons does not grossly impair their development.

Gat1 plays an important role in limiting the buildup of extracellular GABA. Recent studies show that elevating extracellular GABA significantly dampens the excitability of SNc^{DA} axons through activation of presynaptic GABA$_A$Rs and GABA$_B$Rs (Brodnik et al., 2019; Lopes et al., 2019; Roberts et al., 2020; Kramer et al., 2020). Deleting Gat1 from SNc^{DA} neurons may therefore depress their ability to release transmitters indirectly by causing ambient GABA levels to rise. To test this, we estimated extracellular GABA levels in striatum by measuring the amplitude of tonic GABA$_A$R currents in SPNs using the GABA$_A$R blocker picrotoxin. Picrotoxin-mediated shifts in holding current were not different in control and Gat1 cKO^{DA} slices (Figures S4F and S4G), suggesting that ambient GABA levels are comparable between conditions. We also found no differences in the membrane resistance or capacitance of SPNs (Figures S3I and S3J) or in the amplitude and frequency of spontaneous IPSCs (Figures S4H and S4I), indicating that the membrane properties of SPNs and their capacity to detect GABAergic currents are not affected in Gat1 cKO^{DA} mice.

Last, we assessed the integrity of the vesicular release machinery of SNc^{DA} neurons in Gat1 cKO^{DA} mice. Although glutamate release from SNc^{DA} neurons appears intact (Figure 2F), it is anatomically and molecularly distinct from DA release (Fortin et al., 2019; Silm et al., 2019; Zhang et al., 2015). By contrast, DAergic and GABAergic transmission both depend on Vmat2 (Tritsch et al., 2012). We therefore compared the magnitude of DA transients evoked by water rewards in control and Gat1 cKO^{DA} mice using fiber photometry of the DA sensor GRAB-DA$_{2m}$ in striatum (Figure S4J; Sun et al., 2020). As shown in Figures S4K and S4L, reward-evoked DA transients were not smaller in Gat1 cKO^{DA} mice compared with controls, indicating that activity-dependent DA exocytosis is not compromised in SNc^{DA} neurons lacking Gat1. Together, these results point to Gat1 cKO^{DA} mice having a selective deficit in the ability of SNc^{DA} neurons to liberate the transmitter that inhibits SPNs.

Author Manuscript Author Manuscript Author Manuscript Author Manuscript

Inhibitory co-transmission relies on Gat1-mediated import of GABA

Gat1 normally transports GABA from the synaptic cleft into the cytosol (Scimemi, 2014). In SNc^{DA} neurons, Gat1 may therefore serve as a source of GABA for vesicular loading. Alternatively, Gat1 may operate in reverse to mediate non-vesicular GABA efflux (Wu et al., 2007; Bertram et al., 2011), leaving the source of GABA in SNc^{DA} neurons to be identified. Gat1 may also be part of a molecular complex that controls inhibitory signaling from SNc^{DA} neurons independently of its transporter function (Deken et al., 2000; Ryan et al., 2021). To distinguish these possibilities, we selectively expressed constructs in SNc^{DA} neurons to restore inhibitory transmission in Gat1 cKO^{DA} mice.

We first made a Cre-dependent AAV encoding Gat1 tagged with influenza hemagglutinin (HA), which we injected in the midbrain of adult Gat1 cKO^{DA} mice along with ChR2. Immunostaining for HA confirmed our ability to reintroduce Gat1 specifically in SNc^{DA} neurons (Figure 3A). We observed Gat1-HA throughout the axons of SNc^{DA} neurons in dorsal striatum (Figure S5A), consistent with Gat1's usual presynaptic distribution (Uchigashima et al., 2016). Importantly, expressing Gat1-HA in SNc^{DA} neurons of Gat1 cKO^{DA} mice fully restored GABAergic signaling in SPNs (Figures 3C and 3H–3J). Together, these data show that SNc^{DA} neurons remain capable of inhibiting SPNs in adult Gat1 cKO^{DA} mice if provided with Gat1.

To distinguish whether the dependence on Gat1 stems from its ability to transport GABA across the plasma membrane or interact with other molecules, we expressed Gat1-HA with a single amino acid mutation (R69K) that abolishes GABA transport but not membrane expression (Dayan-Alon and Kanner, 2019; Pantanowitz et al., 1993) along with ChR2 in SNc^{DA} neurons of Gat1 cKO^{DA} mice. Despite strong expression of Gat1(R69K)-HA in SNc^{DA} cell bodies and axons (Figures 3A and S5A) and successful activation of SNc^{DA} axons in striatum (Figures S5B–S5E), we were unable to evoke oIPSCs in SPNs (Figures 3D and 3H). This suggests that SNc^{DA} neurons depend on Gat1's transport function to inhibit SPNs.

If Gat1 acts to import GABA for vesicular release, a strong prediction is that other means of supplying cytosolic GABA to SNc^{DA} axons of Gat1 cKO^{DA} mice should also reinstate inhibitory transmission. To test this, we transduced SNc^{DA} neurons of Gat1 cKO^{DA} mice with ChR2 and the cytosolic GABA synthetic enzyme Gad67. Consistent with our prediction, expressing Gad67 in SNc^{DA} neurons lacking Gat1 rescued inhibitory co-transmission (Figures 3E and 3H–3J). We obtained similar results with Gad65 (Figures S5F and S5G), but not with Aldh1a1 (Figures 3F and 3H). Interestingly, oIPSCs evoked from SNc^{DA} neurons expressing Gad65 or Gad67 were significantly less prone to rundown with successive stimulation compared with Gat1-expressing controls (Figure S5H). Together, these experiments show that Gat1 contributes to inhibitory co-transmission by importing GABA into the cytoplasm of SNc^{DA} neurons for vesicular loading.

Synaptic release of GABA from SNc^{DA} neurons depends on Vmat2

We previously suggested using pharmacology that GABAergic transmission from SNc^{DA} neurons requires Vmat2 (Tritsch et al., 2012). However, GABA does not resemble

Author Manuscript Author Manuscript Author Manuscript Author Manuscript

other Vmat2 substrates, raising the possibility that GABA is loaded into synaptic vesicles using another transporter that is sensitive to Vmat2 antagonists. To rule out this possibility, we measured oIPSCs in slices in which ChR2 is expressed genetically in DAergic axons (Madisen et al., 2012) and Vmat2 is genetically knocked down (*Dat*$^{IRES\text{-}Cre/+}$:Ai32$^{+/-}$;*Vmat2*$^{fl/+}$ or Vmat2 cKD^{DA} mice; Figure 4A), as deletion of Vmat2 results in post-natal death (Isingrini et al., 2016). DA release is highly sensitive to Vmat2 levels (Fon et al., 1997). If GABA is similarly dependent on Vmat2 for vesicular transport, we hypothesized that the amplitude of oIPSCs should be depressed in Vmat2 cKD^{DA} mice. Indeed, oIPSCs were 50% smaller compared with controls (Figures 4B and 4C) but otherwise comparable in synaptic latency and kinetics (Figure S6A). By contrast, oEPSCs were unchanged (Figures 4B, 4C, and S6B), indicating that knocking down Vmat2 does not impair the release of transmitters that do not depend on Vmat2 for vesicular loading.

To further implicate Vmat2, we bred the *Vmat2*^{fl} allele in knockin mice expressing Flp recombinase specifically in DAergic neurons (*Dat*$^{IRES\text{-}Flpo}$). Adult mice with no (control; *Dat*$^{IRES\text{-}Flpo/+}$;*Vmat2*$^{+/+}$) or both alleles of *Vmat2* floxed (cKO^{DA}: *Dat*$^{IRES\text{-}Flpo/+}$;*Vmat2*$^{fl/fl}$) were injected unilaterally with two AAVs in SNc; one encoding Flp-dependent Cre and the other Cre-dependent ChR2 (Figure 4D) to restrict Vmat2 deletion and ChR2 expression to SNc^{DA} neurons in the mature nervous system (Figure 4E). Vmat2 cKO^{DA} mice showed strong ipsiversive rotational bias consistent with severe unilateral loss of DA release 16 weeks after viral transduction (Isingrini et al., 2017). We obtained slices from these mice and recorded oIPSCs and oEPSCs from SPNs in dorsal striatum (Figure 4F). ChR2 stimulation reliably evoked oEPSCs of comparable amplitude and kinetics in control and Vmat2 cKO^{DA} mice (Figures 4G and S6C) but failed to evoke oIPSCs in Vmat2 cKO^{DA} slices (Figures 4F and 4G), demonstrating that Vmat2 is essential for inhibitory co-transmission from SNc^{DA} neurons.

To confirm that GABA itself can be a substrate for Vmat2-mediated vesicular loading, we compared oIPSCs recorded in Gat1 cKO^{DA} mice expressing Gad67 in SNc^{DA} neurons in the presence or absence of the Vmat2 antagonist reserpine. We selected these mice, as the inhibitory transmitter released by SNc^{DA} neurons is unquestionably GABA. Compared with untreated slices, reserpine strongly depressed the amplitude of oIPSCs, but not oEPSCs (Figures 4H, 4I, and S6D), providing strong evidence that Vmat2 supports vesicular transport of GABA.

DISCUSSION

In addition to releasing DA, SNc^{DA} neurons exert a rapid and potent inhibitory influence on downstream striatal neurons through synaptic co-release of an inhibitory transmitter, the identity of which has remained speculative (Tritsch et al., 2016). Here, we provide strong evidence that the neurotransmitter that SNc^{DA} neurons co-release is GABA, that Vmat2 is required for vesicular packaging and release of GABA, and that SNc^{DA} neurons sustain inhibitory transmission without producing GABA, relying instead on presynaptic uptake through the membrane GABA transporter Gat1.

Author Manuscript Author Manuscript Author Manuscript Author Manuscript

The chemical identity of a neurotransmitter is traditionally established by determining if a synapse possesses the means to (1) acquire said transmitter, typically by expressing synthetic enzymes, (2) package it into synaptic vesicles, (3) detect it postsynaptically using specific receptors, and (4) terminate its synaptic actions, most commonly through membrane uptake or enzymatic degradation. SNc^{DA} neuron stimulation evokes nanoampere-sized $GABA_AR$ IPSCs in SPNs (Kim et al., 2015; Nelson et al., 2014; Tritsch et al., 2012), the decay kinetics of which are shaped by GABA transporters (Tritsch et al., 2014), suggesting that the released transmitter is GABA. However, this assertion was called into question, as mouse SNc^{DA} neurons lack molecules considered essential for GABA release and rely on a vesicular transporter not known to transport GABA. Here, we show that inhibitory co-transmission from SNc^{DA} neurons is abolished upon selective deletion of Gat1 from DA neurons. We demonstrate that this effect is not secondary to developmental or experimental confounds, as SNc^{DA} neurons remain structurally and functionally competent to co-release DA, glutamate, and even GABA (if GABA is provided to DA neurons through cell-type-specific expression of Gad65 or Gad67). Importantly, we restore inhibitory co-transmission from SNc^{DA} neurons in adult mice by selectively introducing Gat1, Gad67, or Gad65 in SNc^{DA} neurons, but not a GABA transport-deficient Gat1 point-mutant. This indicates that Gat1's transporter function is required for SNc^{DA} neurons to inhibit SPNs and that Gad65 and Gad67 can functionally replace Gat1. Last, we provide fresh genetic evidence that Vmat2 supports the vesicular transport of GABA. When combined with previous reports showing that GABA can be observed in close association with $Vmat2^+$ synaptic vesicles in striatal DA terminals (Stensrud et al., 2014) and that Vgat can substitute for Vmat2 to sustain inhibitory transmission from SNc^{DA} neurons (Tritsch et al., 2012), our results establish that GABA possesses all the necessary attributes to be the transmitter that SNc^{DA} neurons release along with DA and glutamate.

Our results provide important mechanistic insights into GABAergic transmission. First, our study describes a mammalian GABAergic synapse lacking the ability to produce GABA. In mice, GABA is almost exclusively synthetized *de novo* from glutamate by Gad65 and Gad67, with Gad67 accounting for most of the GABA produced (Asada et al., 1996, 1997; Tian et al., 1999). Gad65 and Gad67 are therefore considered critical elements for conferring neurons a GABAergic identity. Our results call for an expansion of this list, as SNc^{DA} neurons rely exclusively on Gat1-mediated uptake as their source of GABA. This mechanism explains why GABA co-release is not detected in primary DA neuron cultures not supplemented with extracellular GABA (Sulzer et al., 1998) and raises the interesting possibility that GABA co-release may vary at individual synapses with extracellular GABA levels and Gat1 transporter activity. More importantly, our findings suggest that the function of GABA transporters extends beyond terminating GABA's actions in the synaptic cleft to include sustaining vesicular filling. Such contribution has proven difficult to dissect at Gad-containing synapses (Bragina et al., 2008; Jensen et al., 2003; Wang et al., 2013).

Second, they reveal that, in the absence of Gat1, SNc^{DA} neurons do not possess GABA for synaptic release. This is at odds with a report claiming that Aldh1a1 produces GABA *de novo* in SNc^{DA} neurons (Kim et al., 2015). However, the manipulations employed were not strictly limited to SNc^{DA} neurons. Our experiments show that GABA co-release is not significantly diminished in $Aldh1a1^{-/-}$ mice and that overexpressing Aldh1a1 in

Author Manuscript Author Manuscript Author Manuscript Author Manuscript

adult SNc^{DA} neurons fails to elevate GABA co-release. Although we did not directly measure Aldh1a1's enzymatic activity, our genetic loss- and gain-of-function manipulations call into question its ability to produce GABA. Indeed, deleting Gat1 from DA neurons abolishes GABA co-release without altering Aldh1a1 expression and overexpressing Gad67 or Gad65 in SNc^{DA} neurons of Gat cKO^{DA} mice restores inhibitory co-transmission onto SPNs, but overexpressing Aldha1 does not. Interfering with Aldh1a1 may modify GABA co-transmission indirectly; Aldh1a1 is widely expressed throughout the brain of humans and mice (Adam et al., 2012; Saunders et al., 2018; Zhang et al., 2014), where it controls numerous biological processes that may impact GABAergic signaling. For instance, Aldh1a1 is one of three enzymes responsible for converting retinal into retinoic acid, an important developmental morphogen and transcriptional regulator (Rhinn and Dollé, 2012). Interfering with Aldh1a1 disrupts the development of DA axons and mu opioid receptorrich patches in striatum (Jacobs et al., 2007; Sgobio et al., 2017; Pan et al., 2019). In DA neurons, loss of Aldh1a1 also leads to the accumulation of toxic DA metabolites and α-synuclein aggregates that may affect GABA release (Anderson et al., 2011; Goldstein et al., 2013; Liu et al., 2014). Last, aldehyde dehydrogenases in astrocytes modulate synaptic transmission by altering extracellular GABA homeostasis and neuronal excitability (Kwak et al., 2020; Jin et al., 2021; Melani and Tritsch, 2021).

Last, although Vgat is typically considered essential for packaging GABA into vesicles, Vgat knockout mice are incompletely deficient in synaptic GABA release (Wojcik et al., 2006), suggesting that other vesicular GABA transporters exist. Our data provide fresh evidence that Vmat2 contributes to vesicular packaging of GABA along with DA. First, we show that inhibitory co-transmission is completely blocked when Vmat2 is conditionally deleted from SNc^{DA} neurons. Second, we report that reserpine blocks the release of GABA produced by Gad67 in Gat1 cKO^{DA} mice. Together, our data redefine the minimal molecular machinery necessary to impart neurons with a GABAergic phenotype and pave the way for studies dissecting the specific contribution of GABA co-release from SNc^{DA} neurons to behavior.

Limitations of the study

Although our study calls into question the ability of Aldh1a1 to synthesize GABA in SNc^{DA} neurons, it does not directly rule out the possibility that Aldh1a1 serves in that capacity in other cells. Our study does not establish whether Vmat2 transports GABA into synaptic vesicles directly or indirectly via interactions with other vesicular proteins and whether DA and GABA are copackaged into the same vesicles or released from distinct presynaptic specializations.

STAR★METHODS

RESOURCE AVAILABILITY

Lead contact—Further information and requests for resources and reagents should be directed to and will be fulfilled by the lead contact, Nicolas X. Tritsch (nicolas.tritsch@nyulangone.org).

Author Manuscript Author Manuscript Author Manuscript Author Manuscript

Materials availability

- Plasmids for viral vectors generated in this study (AAV8.DIO.Aldh1a1, AAV8.DIO.Gat1, AAV8.DIO.Gat1(R69K), AAV8.DIO.Gad65 and AAV8.DIO.Gad67) are deposited to Addgene.
- Gat1^{fl} mice generated in this study were deposited at Jackson Laboratories (strain # 037219 - B6.Cg-Slc6a1<tm1.1Ntrch>/J).

Data and code availability

- All data reported in this paper lead contact are available at https://github.com/TritschLab/Melani-Tritsch-2022.
- This paper does not report original code.
- Any additional information required to reanalyze the data reported in this paper is available from the lead contact upon request.

EXPERIMENTAL MODEL AND SUBJECT DETAILS

Adult mice (8–28 weeks old) of both sexes were used in this study in accordance with protocols approved by the New York University Langone Health Institutional Animal Care and Use Committee (protocol #170123). Mice were housed in groups under a reverse 12 h light-dark cycle (dark from 10 a.m. to 10 p.m.) with ad libitum access to food and water. The following transgenic mice were obtained from the Jackson Laboratory: knock-in mice bearing an internal ribosome entry site (IRES)-linked Cre recombinase gene downstream of the gene *Slc6a3*, which encodes the plasma membrane DA transporter Dat (referred to as *Dat*$^{IRES–Cre}$ mice; strain # 006660), CMV^{Cre} mice (strain # 006054), mice expressing the channelrhodopsin-2/EYFP fusion protein upon exposure to Cre recombinase (referred to as *Rosa26*^{Ai32} mice; strain # 033673), and knock-in mice bearing an IRES-FLPo cassette downstream of *Slc6a3*, (referred to as *Dat*$^{IRES\text{-}Flpo}$ mice, strain # 035436). Mice in which the gene encoding Aldh1a1 is conventionally knocked out (B6.129-*Aldh1a1*^{tm1Gdu}/J; referred to as Aldh1a1$^{-/-}$ mice) were kindly donated by Dr. Huaibin Cai (NIH). Mice with a conditional allele of Vmat2 (referred to as *Vmat2*^{fl}) were kindly donated by Dr. Bruno Giros (McGill University). Transgenic lines were maintained on a C57Bl6/J background (Jackson Laboratory strain # 000664) and bred to one another to generate experimental animals, which were genotyped both in house by the NYU Genotyping Core and by Transnetyx.

METHOD DETAILS

Generation of conditional Gat1 knockout mice—Gat1^{fl} mice were generated by genOway by homologous recombination in mouse embryonic stem (ES) cells. LoxP sites flank exons 2, 3 and 4 of *Slc6a1* (Figures 2A and S3A), which contain the ATG initiation codon, the N-terminal intracellular tail, 2 sodium binding sites essential for GABA transport and 3 of 12 transmembrane domains (Bendahan and Kanner, 1993; Pantanowitz et al., 1993). The targeting vector contained a cassette encoding diphtheria toxin and a neomycin resistance cassette flanked by FRT sites for negative and positive selection of ES cell clones, respectively. Homologous recombination at the intended locus were confirmed by PCR screening and Southern blotting of ES cell clones' genomic DNA (Figure S3B). ES

Author Manuscript Author Manuscript Author Manuscript Author Manuscript

cell clones positive for the knock-in (ki) allele were injected into blastocysts to obtain chimeric males, which were bred to Flp deleter mice to excise the Neomycin selection cassette and generate heterozygous mice carrying the floxed allele of Gat1 (referred to as $Gat1^{fl}$ mice). Crossing these mice with lines expressing Cre recombinase enabled the excision of the loxP-flanked region, resulting in a Gat1 conditional knockout allele (cKO): CMV^{Cre} mice mediate germline recombination to knock Gat1 out throughout the body, while $Da^{IRES\text{-}Cre}$ mice delete Gat1 embryonically from Dat-expressing DA neurons only. The following primers were designed and validated by GenOway for the specific detection $Gat1^{fl}$ and $Gat1^{KO}$ alleles: GAT1-FloxF and GAT1-FloxR yielding 170 bp wild-type and 276 bp conditional knock-out bands (Figure S3C), and GAT1-Flox14F, GAT1-Flox18F and GAT1-Flox15R yielding 211 bp wild-type and 818 bp constitutive knock-out bands (Figure S3D).

Adeno-associated viruses (AAVs)—Cre-dependent AAV viruses were used to selectively transduce midbrain DA neurons with channelrhodopsin 2 (ChR2) and express constructs to rescue GABA co-release in $Dat^{IRES\text{-}Cre/+}$;$Aldh1a1^{-/-}$ and $Dat^{IRES\text{-}Cre/+}$;$Gat1^{fl/fl}$ (Gat1 cKO^{DA}) mice. AAV8.EF1a.DIO.hChR2(H134R)-mCherry was obtained from Addgene (# 20297) and AAV9.hSyn.GRAB_DA2 m was provided by Dr. Yulong Li (Peking University). Flp-dependent AAV virus AAV8.EF1a.fDIO-Cre (Addgene # 121675) was used to selectively express Cre recombinase in DA neurons of $Dat^{IRES\text{-}Flpo/+}$ mice. AAV8.EF1a.DIO.Aldh1a1, AAV8. EF1a.DIO.Gat1, AAV8. EF1a.DIO.Gad65 and AAV8. EF1a.DIO.Gad67 were generated by replacing the coding sequence of ChR2-mCherry in Addgene's plasmid #20297 with the protein-coding sequence for Aldh1a1 (NM_013467.3), Gat1 (NM_178703.4), Gat1(R69K), Gad65 (NM_008078.2) or Gad67 (NM_008077.5), respectively, using Asc1 and Nhe1 restriction sites (Genscript). Three copies of the influenza hemagglutinin (HA) coding sequence were inserted at the C-terminus of all constructs except for Gad65 and Gad67 to facilitate immunohistochemical identification. Plasmids were subsequently packaged into AAVs (serotype 8) by the Boston Children Hospital viral core, stored in undiluted aliquots at −80°C and diluted 2–10X in sterile 0.9% saline immediately prior to intracranial injection. All viral constructs created in this study were deposited at Addgene.

Stereotaxic surgery—For stereotaxic viral injections, mice were anesthetized with isoflurane, placed in an animal stereotaxic frame (David Kopf Instruments) and injected (rate: 100 nL/min) in the right SNc of $Dat^{IRES\text{-}Cre}$ mice with 1 μL of a mix of AAVs (Table S1) encoding Cre-dependent ChR2 (1×10^{12} GC/mL) and either Cre-dependent Aldh1a1 (2.4×10^{10} GC/mL), Gat1 (7.5×10^{11} GC/mL), Gat1(R69K) (5.7×10^{11} GC/mL), Gad65 (1.1×10^{12}), Gad67 (3.2×10^{12}) or saline. $Dat^{IRES\text{-}Flpo/+}$ mice were injected into SNc with 1 μL of a mix of AAVs encoding Flp-dependent Cre recombinase (4.2×10^{11}) and Cre-dependent ChR2 (1×10^{12} GC/mL). The optimal dilution of each AAV was empirically determined to enable strong expression while avoiding toxicity. Working dilutions of AAVs were prepared on ice and loaded into a pulled glass injection micropipette (~100 μm tip; Wiretrol II; Drummond) connected to a syringe pump (Legato 111; KD scientific) fitted with a Hamilton syringe (Gastight 1701N) via PE tubing filled with mineral oil immediately prior to intracranial injection. Injection coordinates for SNc were (from bregma): AP −3.12 mm,

Author Manuscript Author Manuscript Author Manuscript Author Manuscript

ML +1.6 mm and DV −4.2 mm (from pia). For fiber photometry, 250 nL of AAV9-hSyn-GRAB_

DA_{2m} (5.3×10^{12} GC/mL) was injected 2.2 mm below pia into the right dorsal striatum (from bregma: AP, +0.5 mm; ML, +2.0 mm). Mice were allowed to recover for at least 3 weeks prior to electrophysiology. $Dat^{IRES\text{-}Flpo/+}$;$Vmat2^{fl/fl}$ mice were kept for 16 weeks following transduction with Flp-dependent Cre AAV to ensure complete depletion of Vmat2 proteins in SNc^{DA} neurons (Isingrini et al., 2017).

Slice electrophysiology—Acute brain slices and whole-cell voltage-clamp recordings from SPNs were obtained blind to experimental conditions using standard methods, as described previously (Tritsch et al., 2012, 2014). Briefly, mice were anesthetized and perfused with ice-cold artificial cerebrospinal fluid (ACSF) containing (in mM) 125 NaCl, 2.5 KCl, 25 $NaHCO_3$, 2 CaCl2, 1 $MgCl_2$, 1.25 NaH_2PO_4 and 11 glucose (295 mOsm·kg^{-1}). Sagittal slices of striatum (275-μm thick) were subsequently obtained in cold choline-based cutting solution (in mM: 110 choline chloride, 25 $NaHCO_3$, 2.5 KCl, 7 $MgCl_2$, 0.5 $CaCl_2$, 1.25 NaH_2PO_4, 25 glucose, 11.6 ascorbic acid, and 3.1 pyruvic acid) using a Leica VT1200 S vibratome. Following 15 min recovery in ACSF at 34°C, slices were kept at room temperature (20–22°C) until use. All solutions were constantly bubbled with 95% O_2/5% CO_2. For recording, slices were transferred to a Plexiglas chamber mounted on an upright microscope (SliceScope Pro 6000; Scientifica) and imaged through a 40X water-immersion objective (Olympus) with infrared light (780 nm) and differential interference contrast (DIC) optics using a complementary metal-oxide-semiconductor (CMOS) camera (ORCA-spark; Hamamatsu). Slices were held down by a flattened U-shaped platinum wire strung with individual strands of synthetic dental floss fibers and were continually superfused (2–2.5 mL/min) with ACSF at 33–34°C by passing it through a feedback-controlled in-line heater (SH-27B; Warner Instruments) before entering the chamber. Whole-cell voltage-clamp recordings were established from SPNs in dorsal striatum identified visually and electrophysiologically. For oIPSC/oEPSC recordings, patch pipettes (2–3 MΩ) were filled with a cesium-based low-chloride internal solution containing (in mM): 135 $CsMeSO_3$, 10 HEPES, 1 EGTA, 3.3 QX-314 (Cl salt), 4 Mg-ATP, 0.3 Na-GTP, 8 Na_2-phosphocreatine (pH 7.3 adjusted with CsOH; 295 mOsm·kg^{-1}). Under these conditions, $GABA_AR$ currents can be isolated as outward currents when SPNs are held at 0 mV, while glutamatergic currents can be isolated as inward currents at E_{Cl} = −70 mV. Inward tonic GABAergic currents and sIPSC in Figure S4 were recorded at −70 mV using an internal solution containing (in mM) 125 CsCl, 10 TEA-Cl, 10 HEPES, 0.1 Cs-EGTA, 3.3 QX-314 (Cl–salt), 4 Mg-ATP, 0.3 Na-GTP, 8 Na_2-Phosphocreatine (pH 7.3 adjusted with CsOH; 295 mOsm) in the presence of NBQX, R-CPP, and CGP55845. For all voltage-clamp experiments, errors due to the voltage drop across the series resistance (<20 MΩ) were left uncompensated. Membrane potentials were corrected for a ~7 mV liquid junction potential. To activate ChR2-expressing SNc^{DA} axons, 1 ms-long full-field pulses of light from a 473-nm LED (p300 CoolLED) were delivered through the objective (10 mW.mm^{-2} under the objective) at 30 s intervals.

Pharmacological reagents—Drugs (all from Tocris) were applied by bath perfusion: SR95531 (10 μM), picrotoxin (100 μM), CGP55845 (5 μM), 2,3-dihydroxy-6-nitro-7-

Author Manuscript Author Manuscript Author Manuscript Author Manuscript

sulfamoylbenzo(f)quinoxaline (NBQX; 10 μM), R,S-3-(2-carboxypiperazin-4-yl)propyl-1-phosphonic acid (R-CPP; 10 μM). To inhibit monoaminergic vesicular transport and deplete transmitter-filled vesicles, mice were injected intraperitoneally with the irreversible Vmat inhibitor reserpine (5 $mg.kg^{-1}$) 24 h and 2 h before slicing. Brain sections from these animals were prepared as described above, but were incubated and recorded in ACSF containing 1 μM reserpine.

Fiber photometry—Upon stereotaxic injection of AAV9.hSyn.GRAB-DA_{2m} in dorso-lateral striatum, a 400 μm optic fiber (FP400URT, Thorlabs) housed in a 1.25 mm ceramic ferrule (CFLC440, Thorlabs) was implanted 0.2 mm above the injection site using C&B metabond (Parkel). Following 2 weeks of recovery in their home cage, mice were habituated for a minimum of 5 days to locomote while head-fixed on a cylindrical wheel placed into a dark soundproof chamber and were water restricted to incite consumption of water rewards delivered from a spout at semi-random 8 to 12 s intervals. Licking was monitored by a capacitive touch sensor (AT42QT1010; Sparkfun). Extracellular DA levels in striatum were imaged by providing 470 nm excitation light from a LED (M470F3; Thorlabs) coupled to an optical fiber (400 μm, 0.48 NA; Doric) to a fluorescence mini-cube (FMC3_E(460–490)_F(500–550)_S; Doric) connected to the mouse via a fiber optic patch cord (400 μm, 0.48 NA; Doric) and zirconia sleeve. Emission light (500–550 nm) was collected through the same patch cord and mini-cube by a femtowatt photoreceiver (2151; Newport) fitted with a FC adapter (FOA_2151_FC; Doric) via a 600 mm 0.48NA fiber optic (Doric).

Immunohistochemistry—Mice were deeply anesthetized with isoflurane and perfused transcardially with 4% paraformaldehyde in 0.1 M sodium phosphate buffer. Brains were post-fixed for 1–3 days, sectioned coronally (50 μm in thickness) using a vibratome (Leica; VT1000S) and processed for immunofluorescence staining for tyrosine hydroxylase (Millipore; AB152, 1:2000), Gat1 (Cell Signaling; 37342, 1:200), Aldh1a1 (R&D Systems; AF5869, 1:200), HA (Abcam; ab18181, 1:500) or Cre (Synaptic Systems; 257 004, 1:500). After primary antibodies incubation (4°C, overnight), the following secondary antibodies (all from Thermo Fisher Scientific) were applied for 2 h at room temperature: Goat anti-mouse IgG Alexa Fluor 568 (A11004), Goat anti-mouse IgG Alexa Fluor 488 (A11029), Goat anti-rabbit IgG Alexa Fluor 488 (A11034), Goat anti-rabbit IgG Alexa Fluor 568 (A11036), Donkey anti-goat IgG Alexa Fluor 568 (A11057), Donkey anti-rabbit IgG Alexa Fluor 488 (A21206). Brain sections were mounted on Superfrost slides and coverslipped with DAPI Fluoromount-G (SouthernBiotech; 0100-20).

***In situ* hybridization—**Mice were deeply anesthetized with isoflurane, the brain was rapidly extracted and frozen on dry ice in plastic cryomolds containing OCT compound (Fisher Scientific; 4585). Coronal sections (16 mm in thickness) were obtained using a Leica CM3050S cryostat, immediately mounted onto Superfrost Plus glass slides (Fisher Scientific; 1255015) and kept at −80°C until use. RNAscope assay was performed following Advanced Cell Diagnostic (ACD) manual Fluorescent Multiplex Kit. Briefly, slides were fixed in ice-cold 4% PFA for 15 min, then dehydrated in 50%, 70% and 100% ethanol before incubation with protease IV at room temperature for 30 min. The following target probes were used: *Slc6a3*/Dat (31544-C2), *Th*/TH (317621), *Gad1*/Gad67 (400951-C3),

Author Manuscript Author Manuscript Author Manuscript Author Manuscript

Gad2/Gad65 (439371-C2). For *Slc6a1*/Gat1, a custom probe was designed by ACD targeting 243–718 bp of NM_178703.4. After the last wash step, sections were incubated in DAPI at room temperature for 30 s before coverslipping with Fluoromount-G (SouthernBiotech; 0100-01).

QUANTIFICATION AND STATISTICAL ANALYSIS

Data acquisition—Membrane currents were amplified and low-pass filtered at 2 kHz using a Multiclamp 700B amplifier (Molecular Devices), digitized at 10 kHz using National Instruments acquisition boards (BNC 2110) and a custom version of ScanImage (Pologruto et al., 2003 https://github.com/bernardosabatinilab/SabalabSoftware_Nov2009) written in MATLAB (Mathworks). Electrophysiology data were analyzed offline using Igor Pro 6.02A (Wavemetrics). In figures, voltage-clamp traces represent the averaged waveform of 3–5 consecutive acquisitions. Single waveforms aligned to optogenetic light stimulus onset were used to measure postsynaptic current peak amplitude, latency (from light onset to current onset), and 10–90% rise time. Only oIPSCs and oEPSCs larger than 11 pA in amplitude were considered to compute prevalence, latency and rise time. For sIPSCs, the detection threshold was set to 20 pA to facilitate event detection in the presence of large and noisy tonic GABA currents. For photometry, signals were continuously digitized at 2 kHz using a National Instruments acquisition board (USB-6343) and Wavesurfer software (Janelia), low-pass filtered and down-sampled to 30 Hz, and aligned to the first lick within 500 ms of water delivery for analysis in MATLAB. For *in situ* hybridization and immunofluorescence analyses, brain sections were first digitized with an Olympus VS120 slide-scanning microscope. High-resolution images of regions of interest were subsequently acquired with a Zeiss LSM 800 confocal microscope. Confocal images in figures represent maximum intensity projections of 3 μm-thick confocal stacks. To estimate the number of DA neurons in control and Gat1 cKO^{DA} mice (Figure S4), we used Cellpose (Stringer et al., 2021) to automatically segment the cell bodies of TH$^+$ neurons in confocal images of ventral midbrain. We report the mean number of TH$^+$ cells counted per mouse across the 3 evenly-spaced coronal sections of SNc (−2.9, −3.1, −3.3 mm AP, from bregma). We calculated the mean fluorescence intensity of TH and Aldh1a1 in DA neurons in ImageJ (Schindelin et al., 2012) using the masks to obtained with CellPose. The fraction of TH$^+$ cells that are Aldh1a1$^+$ was estimated by counting the fraction of TH$^+$ cell masks where Aldh1a1 fluorescence intensity exceeded a threshold common to all sections. DA axon density was calculated as the mean percentage of dorsal striatal neuropil (excluding neuronal somata and corticofugal axon bundles) covered by TH+ axons across 4 coronal sections (0.75, 0.65, 0.55, 0.45 mm AP, from bregma) per mouse.

Statistical analysis—Data (reported in text and figures as mean ± SEM) were compared using Prism 9 (GraphPad) with the following non-parametric statistical tests (as indicated in the text): Mann-Whitney for comparisons between test and control groups, and Kruskal–Wallis analysis of variance (ANOVA) followed by Dunn's Multiple Comparison Test for multiple group comparisons. Two-way repeated measures ANOVA were used in experiment characterizing the time course of synaptic transmission rundown (Figure S5H). For electrophysiology experiments, n-values represent the number of recorded cells. In most cases, a single cell was recorded per slice, with each animal contributing at most 5

Author Manuscript Author Manuscript Author Manuscript Author Manuscript

individual recordings per condition. For immunohistochemistry, n represents the number of mice analyzed (Figures S4B–S4D) or the total number of TH^+ cells quantified (Figure S4E). For fiber photometry recordings, n represents the number of imaging sessions performed, with a maximum of 2 imaging sessions per mouse. Exact p-values are provided in text and figure legends, and statistical significance in figures is presented as *p < 0.05, **p < 0.01 and ***p < 0.001.

Supplementary Material

Refer to Web version on PubMed Central for supplementary material.

ACKNOWLEDGMENTS

We thank Adam Carter, Margaret Rice, Dick Tsien, and members of the Tritsch laboratory for comments on the manuscript; Yulong Li for the GRAB-DA_{2m} DA sensor; and Huaibin Cai and Bruno Giros for kindly providing the Aldh1a1$^{-/-}$ and VMAT2$^{f/f}$ mice, respectively. We acknowledge the New York University Medical Center Rodent Genetic Engineering Laboratory for rederivation, the Genotyping Core Laboratory for mouse genotyping, the Department of Comparative Medicine for animal care and maintenance, and the Neuroscience Institute's imaging facilities for microscope availability. R.M. is supported by a Marlene and Paolo Fresco Postdoctoral Fellowship. N.X.T. is an Alfred P. Sloan Research Fellow in Neuroscience and is supported by grants from the Dana, Whitehall and Feldstein Medical Foundations, as well as from the National Institutes of Health (DP2NS105553).

REFERENCES

Adam SA, Schnell O, Pöschl J, Eigenbrod S, Kretzschmar HA, Tonn J-C, and Schüller U (2012). ALDH1A1 is a marker of astrocytic differentiation during brain development and correlates with better survival in glioblastoma patients. Brain Pathol. 22, 788–797. [PubMed: 22417385]

Anderson DW, Schray RC, Duester G, and Schneider JS (2011). Functional significance of aldehyde dehydrogenase ALDH1A1 to the nigrostriatal dopamine system. Brain Res. 1408, 81–87. [PubMed: 21784415]

Asada H, Kawamura Y, Maruyama K, Kume H, Ding R, Ji FY, Kanbara N, Kuzume H, Sanbo M, Yagi T, et al. (1996). Mice lacking the 65 kDa isoform of glutamic acid decarboxylase (GAD65) maintain normal levels of GAD67 and GABA in their brains but are susceptible to seizures. Biochem. Biophys. Res. Commun. 229, 891–895. [PubMed: 8954991]

Asada H, Kawamura Y, Maruyama K, Kume H, Ding RG, Kanbara N, Kuzume H, Sanbo M, Yagi T, and Obata K (1997). Cleft palate and decreased brain gamma-aminobutyric acid in mice lacking the 67-kDa isoform of glutamic acid decarboxylase. Proc. Natl. Acad. Sci. U S A 94, 6496–6499. [PubMed: 9177246]

Bäckman CM, Malik N, Zhang Y, Shan L, Grinberg A, Hoffer BJ, Westphal H, and Tomac AC (2006). Characterization of a mouse strain expressing Cre recombinase from the 3' untranslated region of the dopamine transporter locus. Genesis 44, 383–390. [PubMed: 16865686]

Belelli D, and Lambert JJ (2005). Neurosteroids: endogenous regulators of the GABA(A) receptor. Nat. Rev. Neurosci. 6, 565–575. [PubMed: 15959466]

Bendahan A, and Kanner BI (1993). Identification of domains of a cloned rat brain GABA transporter which are not required for its functional expression. FEBS Lett. 318, 41–44. [PubMed: 8436223]

Bertram S, Cherubino F, Bossi E, Castagna M, and Peres A (2011). GABA reverse transport by the neuronal cotransporter GAT1: influence of internal chloride depletion. Am. J. Physiol. Cell Physiol. 301, C1064–C1073. [PubMed: 21775701]

Bragina L, Marchionni I, Omrani A, Cozzi A, Pellegrini-Giampietro DE, Cherubini E, and Conti F (2008). GAT-1 regulates both tonic and phasic GABA(A) receptor-mediated inhibition in the cerebral cortex. J. Neurochem. 105, 1781–1793. [PubMed: 18248614]

Brodnik ZD, Batra A, Oleson EB, and España RA (2019). Local GABAA receptor-mediated suppression of dopamine release within the nucleus accumbens. ACS Chem. Neurosci. 10, 1978–1985. [PubMed: 30253088]

Author Manuscript Author Manuscript Author Manuscript Author Manuscript

Dayan-Alon O, and Kanner BI (2019). Internal gate mutants of the GABA transporter GAT1 are capable of substrate exchange. Neuropharmacology 161, 107534. [PubMed: 30790582]

Deken SL, Beckman ML, Boos L, and Quick MW (2000). Transport rates of GABA transporters: regulation by the N-terminal domain and syntaxin 1A. Nat. Neurosci. 3, 998–1003. [PubMed: 11017172]

Eskenazi D, Malave L, Mingote S, Yetnikoff L, Ztaou S, Velicu V, Rayport S, and Chuhma N (2021). Dopamine neurons that cotransmit glutamate, from synapses to circuits to behavior. Front. Neural Circuits 15, 40.

Fan X, Molotkov A, Manabe S-I, Donmoyer CM, Deltour L, Foglio MH, Cuenca AE, Blaner WS, Lipton SA, and Duester G (2003). Targeted disruption of Aldh1a1 (Raldh1) provides evidence for a complex mechanism of retinoic acid synthesis in the developing retina. Mol. Cell Biol. 23, 4637–4648. [PubMed: 12808103]

Fon EA, Pothos EN, Sun B-C, Killeen N, Sulzer D, and Edwards RH (1997). Vesicular transport regulates monoamine storage and release but is not essential for amphetamine action. Neuron 19, 1271–1283. [PubMed: 9427250]

Fortin GM, Ducrot C, Giguére N, Kouwenhoven WM, Bourque M-J, Pacelli C, Varaschin RK, Brill M, Singh S, Wiseman PW, et al. (2019). Segregation of dopamine and glutamate release sites in dopamine neuron axons: regulation by striatal target cells. FASEB J. 33, 400–417. [PubMed: 30011230]

Goldstein DS, Sullivan P, Holmes C, Miller GW, Alter S, Strong R, Mash DC, Kopin IJ, and Sharabi Y (2013). Determinants of buildup of the toxic dopamine metabolite DOPAL in Parkinson's disease. J. Neurochem. 126, 591–603. [PubMed: 23786406]

Hnasko TS, Chuhma N, Zhang H, Goh GY, Sulzer D, Palmiter RD, Rayport S, and Edwards RH (2010). Vesicular glutamate transport promotes dopamine storage and glutamate corelease *in vivo*. Neuron 65, 643–656. [PubMed: 20223200]

Isingrini E, Guinaudie C, C Perret L, Rainer Q, Moquin L, Gratton A, and Giros B (2017). Genetic elimination of dopamine vesicular stocks in the nigrostriatal pathway replicates Parkinson's disease motor symptoms without neuronal degeneration in adult mice. Sci. Rep. 7, 12432. [PubMed: 28963508]

Isingrini E, Perret L, Rainer Q, Sagueby S, Moquin L, Gratton A, and Giros B (2016). Selective genetic disruption of dopaminergic, serotonergic and noradrenergic neurotransmission: insights into motor, emotional and addictive behaviour. J. Psychiatry Neurosci. 41, 169–181. [PubMed: 26505143]

Jacobs FMJ, Smits SM, Noorlander CW, von Oerthel L, van der Linden AJA, Burbach JPH, and Smidt MP (2007). Retinoic acid counteracts developmental defects in the substantia nigra caused by Pitx3 deficiency. Development 134, 2673–2684. [PubMed: 17592014]

Jensen K, Chiu C-S, Sokolova I, Lester HA, and Mody I (2003). GABA transporter-1 (GAT1)-deficient mice: differential tonic activation of GABAA versus GABAB receptors in the hippocampus. J. Neurophysiol. 90, 2690–2701. [PubMed: 12815026]

Jin S, Cao Q, Yang F, Zhu H, Xu S, Chen Q, Wang Z, Lin Y, Cinar R, Pawlosky RJ, et al. (2021). Brain ethanol metabolism by astrocytic ALDH2 drives the behavioural effects of ethanol intoxication. Nat. Metab 3, 337–351. [PubMed: 33758417]

Johnston GA (1996). GABAA receptor pharmacology. Pharmacol. Ther. 69, 173–198. [PubMed: 8783370]

Kim J-I, Ganesan S, Luo SX, Wu Y-W, Park E, Huang EJ, Chen L, and Ding JB (2015). Aldehyde dehydrogenase 1a1 mediates a GABA synthesis pathway in midbrain dopaminergic neurons. Science 350, 102–106. [PubMed: 26430123]

Kramer PF, Twedell EL, Shin JH, Zhang R, and Khaliq ZM (2020). Axonal mechanisms mediating g-aminobutyric acid receptor type A (GABA-A) inhibition of striatal dopamine release. eLife 9, e55729. [PubMed: 32870779]

Kwak H, Koh W, Kim S, Song K, Shin J-I, Lee JM, Lee EH, Bae JY, Ha GE, Oh J-E, et al. (2020). Astrocytes control sensory acuity via tonic inhibition in the thalamus. Neuron 108, 691–706.e10. [PubMed: 32905785]

Author Manuscript Author Manuscript Author Manuscript Author Manuscript

Liu G, Yu J, Ding J, Xie C, Sun L, Rudenko I, Zheng W, Sastry N, Luo J, Rudow G, et al. (2014). Aldehyde dehydrogenase 1 defines and protects a nigrostriatal dopaminergic neuron subpopulation. J. Clin. Invest 124, 3032–3046. [PubMed: 24865427]

Lopes EF, Roberts BM, Siddorn RE, Clements MA, and Cragg SJ (2019). Inhibition of nigrostriatal dopamine release by striatal GABAA and GABAB receptors. J. Neurosci. 39, 1058–1065. [PubMed: 30541909]

Madisen L, Mao T, Koch H, Zhuo J, Berenyi A, Fujisawa S, Hsu Y-WA, Garcia AJ, Gu X, Zanella S, et al. (2012). A toolbox of Cre-dependent optogenetic transgenic mice for light-induced activation and silencing. Nat. Neurosci. 15, 793–802. [PubMed: 22446880]

McCaffery P, and Dräger UC (1994). High levels of a retinoic acid-generating dehydrogenase in the meso-telencephalic dopamine system. Proc. Natl. Acad. Sci. U S A 91, 7772–7776. [PubMed: 8052659]

Melani R, and Tritsch NX (2021). How alcohol affects motor control: not your usual suspects. Nat. Metab. 3, 293–294. [PubMed: 33758418]

Nelson AB, Hammack N, Yang CF, Shah NM, Seal RP, and Kreitzer AC (2014). Striatal cholinergic interneurons Drive GABA release from dopamine terminals. Neuron 82, 63–70. [PubMed: 24613418]

Pan J, Yu J, Sun L, Xie C, Chang L, Wu J, Hawes S, Saez-Atienzar S, Zheng W, Kung J, et al. (2019). ALDH1A1 regulates postsynaptic m-opioid receptor expression in dorsal striatal projection neurons and mitigates dyskinesia through transsynaptic retinoic acid signaling. Sci. Rep. 9, 3602. [PubMed: 30837649]

Pantanowitz S, Bendahan A, and Kanner BI (1993). Only one of the charged amino acids located in the transmembrane alpha-helices of the gamma-aminobutyric acid transporter (subtype A) is essential for its activity. J. Biol. Chem. 268, 3222–3225. [PubMed: 8428999]

Pologruto TA, Sabatini BL, and Svoboda K (2003). ScanImage: flexible software for operating laser scanning microscopes. Biomed. Eng. Online 2, 13. [PubMed: 12801419]

Poulin J-F, Zou J, Drouin-Ouellet J, Kim K-YA, Cicchetti F, and Awatramani RB (2014). Defining midbrain dopaminergic neuron diversity by single-cell gene expression profiling. Cell Rep. 9, 930–943. [PubMed: 25437550]

Rhinn M, and Dollé P (2012). Retinoic acid signalling during development. Developement 139, 843–858.

Roberts BM, Doig NM, Brimblecombe KR, Lopes EF, Siddorn RE, Threlfell S, Connor-Robson N, Bengoa-Vergniory N, Pasternack N, Wade-Martins R, et al. (2020). GABA uptake transporters support dopamine release in dorsal striatum with maladaptive downregulation in a parkinsonism model. Nat. Commun. 11, 4958. [PubMed: 33009395]

Ryan RM, Ingram SL, and Scimemi A (2021). Regulation of glutamate, GABA and dopamine transporter uptake, surface mobility and expression. Front. Cell. Neurosci. 15, 670346. [PubMed: 33927596]

Saunders A, Macosko EZ, Wysoker A, Goldman M, Krienen FM, de Rivera H, Bien E, Baum M, Bortolin L, Wang S, et al. (2018). Molecular diversity and specializations among the cells of the adult mouse brain. Cell 174, 1015–1030.e16. [PubMed: 30096299]

Schindelin J, Arganda-Carreras I, Frise E, Kaynig V, Longair M, Pietzsch T, Preibisch S, Rueden C, Saalfeld S, Schmid B, et al. (2012). Fiji: an open-source platform for biological-image analysis. Nat Methods 9, 676–682. [PubMed: 22743772]

Schwenk F, Baron U, and Rajewsky K (1995). A cre -transgenic mouse strain for the ubiquitous deletion of loxP -flanked gene segments including deletion in germ cells. Nucleic Acids Research 23 (24), 5080–5081. [PubMed: 8559668]

Scimemi A (2014). Structure, function, and plasticity of GABA transporters. Front. Cell. Neurosci 8, 161. [PubMed: 24987330]

Sgobio C, Wu J, Zheng W, Chen X, Pan J, Salinas AG, Davis MI, Lovinger DM, and Cai H (2017). Aldehyde dehydrogenase 1-positive nigrostriatal dopaminergic fibers exhibit distinct projection pattern and dopamine release dynamics at mouse dorsal striatum. Sci. Rep. 7, 5283. [PubMed: 28706191]

Author Manuscript Author Manuscript Author Manuscript Author Manuscript

Silm K, Yang J, Marcott PF, Asensio CS, Eriksen J, Guthrie DA, Newman AH, Ford CP, and Edwards RH (2019). Synaptic vesicle recycling pathway determines neurotransmitter content and release properties. Neuron 102, 786–800.e5. [PubMed: 31003725]

Stensrud MJ, Puchades M, and Gundersen V (2014). GABA is localized in dopaminergic synaptic vesicles in the rodent striatum. Brain Struct. Funct. 219, 1901–1912. [PubMed: 23851655]

Stringer C, Wang T, Michaelos M, and Pachitariu M (2021). Cellpose: a generalist algorithm for cellular segmentation. Nat. Methods 18, 100–106. [PubMed: 33318659]

Sulzer D, Joyce MP, Lin L, Geldwert D, Haber SN, Hattori T, and Rayport S (1998). Dopamine neurons make glutamatergic synapses *in vitro*. J. Neurosci. 18, 4588–4602. [PubMed: 9614234]

Sun F, Zhou J, Dai B, Qian T, Zeng J, Li X, Zhuo Y, Zhang Y, Wang Y, Qian C, et al. (2020). Next-generation GRAB sensors for monitoring dopaminergic activity *in vivo*. Nat. Methods 17, 1156–1166. [PubMed: 33087905]

Tecuapetla F, Patel JC, Xenias H, English D, Tadros I, Shah F, Berlin J, Deisseroth K, Rice ME, Tepper JM, et al. (2010). Glutamatergic signaling by mesolimbic dopamine neurons in the nucleus accumbens. J. Neurosci. 30, 7105–7110. [PubMed: 20484653]

Tian N, Petersen C, Kash S, Baekkeskov S, Copenhagen D, and Nicoll R (1999). The role of the synthetic enzyme GAD65 in the control of neuronal g-aminobutyric acid release. Proc. Natl. Acad. Sci. U S A 96, 12911–12916. [PubMed: 10536022]

Tritsch NX, Ding JB, and Sabatini BL (2012). Dopaminergic neurons inhibit striatal output through non-canonical release of GABA. Nature 490, 262–266. [PubMed: 23034651]

Tritsch NX, Granger AJ, and Sabatini BL (2016). Mechanisms and functions of GABA co-release. Nat. Rev. Neurosci. 17, 139–145. [PubMed: 26865019]

Tritsch NX, Oh W-J, Gu C, and Sabatini BL (2014). Midbrain dopamine neurons sustain inhibitory transmission using plasma membrane uptake of GABA, not synthesis. eLife 3, e01936. [PubMed: 24843012]

Trudeau L-E, Hnasko TS, Wallén-Mackenzie A, Morales M, Rayport S, and Sulzer D (2014). The multilingual nature of dopamine neurons. Prog. Brain Res. 211, 141–164. [PubMed: 24968779]

Uchigashima M, Ohtsuka T, Kobayashi K, and Watanabe M (2016). Dopamine synapse is a neuroligin-2-mediated contact between dopaminergic presynaptic and GABAergic postsynaptic structures. Proc. Natl. Acad. Sci. U S A 113, 4206–4211. [PubMed: 27035941]

Wang L, Tu P, Bonet L, Aubrey KR, and Supplisson S (2013). Cytosolic transmitter concentration regulates vesicle cycling at hippocampal GABAergic terminals. Neuron 80, 143–158. [PubMed: 24094108]

Wojcik SM, Katsurabayashi S, Guillemin I, Friauf E, Rosenmund C, Brose N, and Rhee J-S (2006). A shared vesicular carrier allows synaptic corelease of GABA and glycine. Neuron 50, 575–587. [PubMed: 16701208]

Wu Y, Wang W, Díez-Sampedro A, and Richerson GB (2007). Nonvesicular inhibitory neurotransmission via reversal of the GABA transporter GAT-1. Neuron 56, 851–865. [PubMed: 18054861]

Yelin R, and Schuldiner S (1995). The pharmacological profile of the vesicular monoamine transporter resembles that of multidrug transporters. FEBS Lett. 377, 201–207. [PubMed: 8543051]

Zhang S, Qi J, Li X, Wang H-L, Britt JP, Hoffman AF, Bonci A, Lupica CR, and Morales M (2015). Dopaminergic and glutamatergic microdomains in a subset of rodent mesoaccumbens axons. Nat. Neurosci. 18, 386–392. [PubMed: 25664911]

Zhang Y, Chen K, Sloan SA, Bennett ML, Scholze AR, O'Keeffe S, Phatnani HP, Guarnieri P, Caneda C, Ruderisch N, et al. (2014). An RNA-sequencing transcriptome and splicing database of glia, neurons, and vascular cells of the cerebral cortex. J. Neurosci. 34, 11929–11947. [PubMed: 25186741]

Author Manuscript Author Manuscript Author Manuscript Author Manuscript

Highlights

- SNc^{DA} neurons release GABA through unconventional mechanisms
- Aldh1a1 is neither necessary nor sufficient to provide GABA in SNc^{DA} neurons
- Selective deletion of Gat1 from SNc^{DA} neurons abolishes GABA co-release
- Selective deletion of Vmat2 from SNc^{DA} neurons abolishes GABA co-release

Author Manuscript Author Manuscript Author Manuscript Author Manuscript

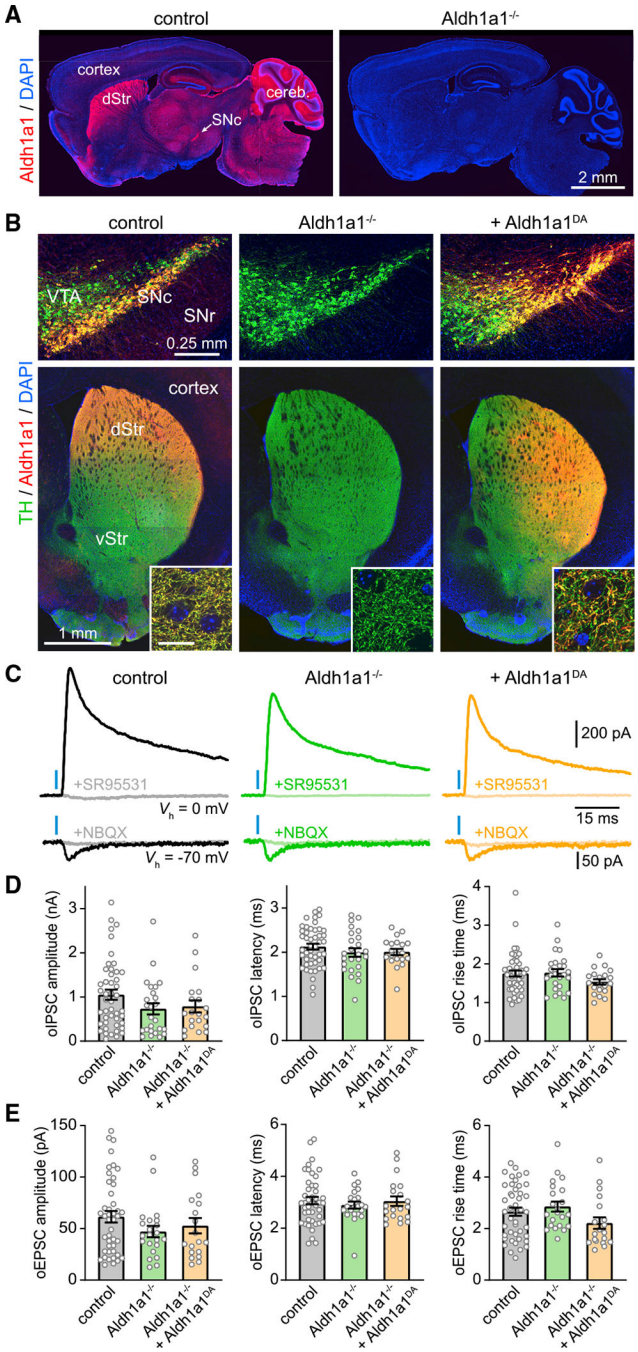

Figure 1. Aldh1a1 does not contribute to GABA co-release from DA neurons

(A) Sagittal sections from control (left) and Aldh1a1$^{-/-}$ (right) mice immunolabeled for Aldh1a1 (red) and DAPI nuclear stain (blue). dStr, dorsal striatum; Cereb, cerebellum.

(B) Coronal brain sections from a control *Dat*$^{IRES\text{-}Cre/+}$ mouse (left), a *Dat*$^{IRES\text{-}Cre/+}$;Aldh1a1$^{-/-}$ mouse (middle), and a *Dat*$^{IRES\text{-}Cre/+}$;Aldh1a1$^{-/-}$ mouse in which Aldh1a1 is selectively restored in DA neurons (right) immunolabeled for TH (green), Aldh1a1 (red), and DAPI (blue). Top: confocal image of SNc, ventral tegmental area (VTA),

Author Manuscript Author Manuscript Author Manuscript Author Manuscript

and substantia nigra pars reticulata (SNr). Bottom: epifluorescence image of striatum. vStr, ventral striatum. Inset: confocal detail in dorsal striatum (scale, 10 μm).

(C) Postsynaptic responses recorded from SPNs voltage-clamped (V_h) at 0 (top) or −70 mV (bottom) upon stimulation of SNc^{DA} axons (blue bar) before and after application of the $GABA_AR$ antagonist SR95531 (10 μM) or the ionotropic glutamate receptor blockers NBQX (10 μM).

(D) Mean amplitude (left), synaptic latency (middle), and 10% to 90% rise time (right) of oIPSCs recorded from SPNs in slices from control (n = 46), $Aldh1a1^{-/-}$ (n = 25), and $Aldh1a1^{-/-}$ mice expressing Aldh1a1 in SNc^{DA} neurons (n = 20; amplitude: p = 0.16; latency: p = 0.41; rise time: p = 0.17; Kruskal-Wallis). Individual values shown along with population mean ± SEM.

(E) Same as (D) for oEPSCs (amplitude: p = 0.338; latency: p = 0.94; rise time: p = 0.07; Kruskal-Wallis).

Author Manuscript Author Manuscript Author Manuscript Author Manuscript

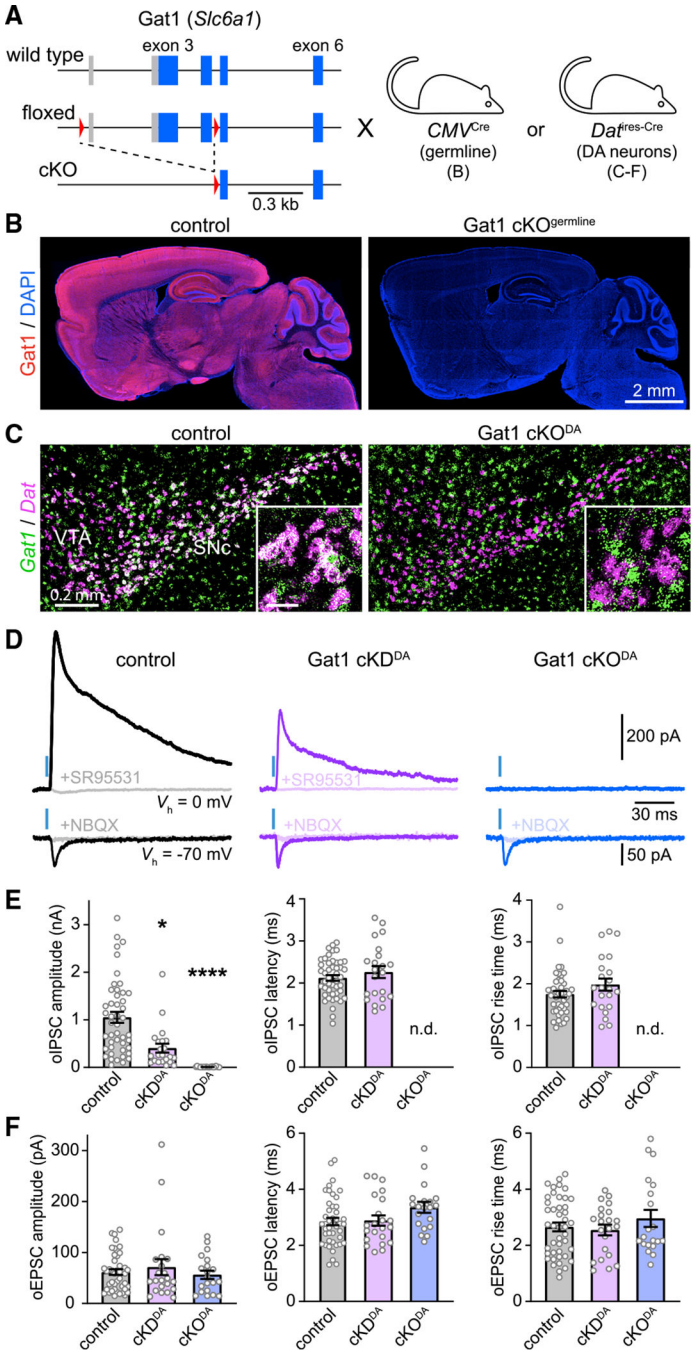

Figure 2. GABAergic co-transmission from SNc^{DA} neurons is abolished in Gat1 cKO^{DA} mice

(A) Schematic of Gat1 locus (top), floxed allele before (middle) and after (bottom) Cre-mediated excision in *CMV*^{Cre} or *Dat*$^{IRES\text{-}Cre}$ mice. Boxes: exons with protein-coding regions in blue; red triangles: LoxP sites.

(B) Sagittal brain sections from control (left) and Gat1 cKO^{germline} mice (right) immunolabeled for Gat1 (red) and DAPI (blue).

(C) Fluorescence *in situ* hybridization for *Gat1* (green) and *Dat* (magenta; labels DA neurons) in coronal brain sections from control (*Dat*$^{IRES\text{-}Cre/+}$;*Gat1*$^{+/+}$; left) and Gat1

Author Manuscript Author Manuscript Author Manuscript Author Manuscript

cKO^{DA} (*Dat*$^{IRES\text{-}Cre/+}$;*Gat1*$^{fl/fl}$; right) mice. Colocalization appears white. Inset: detail (scale, 50 μm).

(D) Example oIPSCs (top) and oEPSCs (bottom) in SPNs held at 0 and −70 mV, respectively, in *Dat*$^{IRES\text{-}Cre/+}$ mice with no (control; black), one (cKD^{DA}; purple), or both (cKO^{DA}; blue) alleles of Gat1 conditionally deleted from SNc^{DA} neurons before and after application of SR95531 (10 μM) or NBQX (10 μM).

(E) Meanamplitude(left), synaptic latency (middle), and 10% to 90% rise time (right) of oIPSCs recorded from SPNs in control (n = 46), cKD^{DA} (n = 22), and cKO^{DA} (n = 22) slices (amplitude: $p = 2.94 \times 10^{-13}$; Kruskal-Wallis; *p = 0.012, ***$p = 1.01 \times 10^{-13}$ versus control, Dunn's multiple comparison; latency: p = 0.65; rise time: p = 0.18 between control and Gat1 cKD^{DA}; Mann-Whitney). nd, not detected. Individual values shown along with population mean ± SEM.

(F) Same as (E) for oEPSCs (amplitude: p = 0.85; latency: p = 0.18; rise time: p = 0.76; Kruskal-Wallis).

Author Manuscript Author Manuscript Author Manuscript Author Manuscript

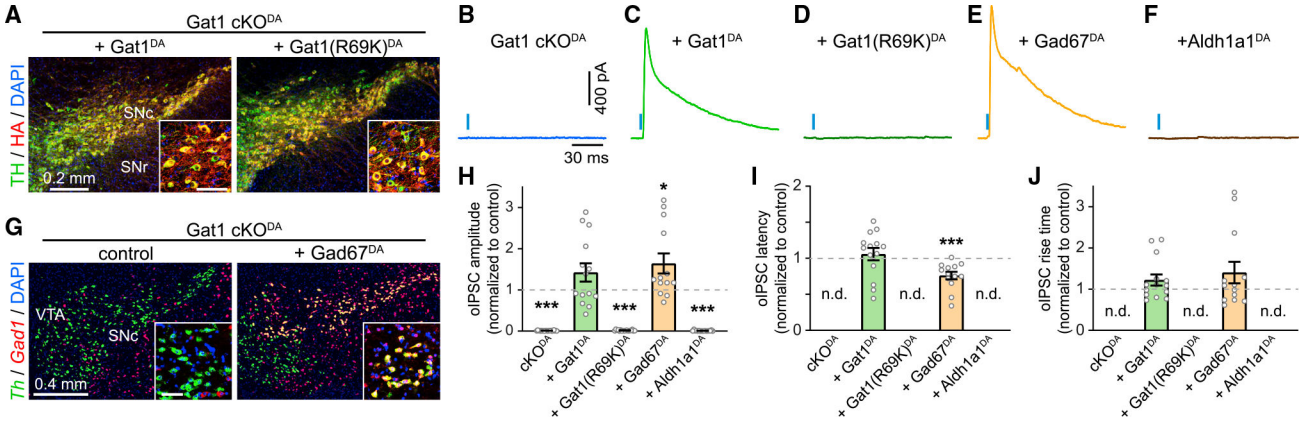

Figure 3. GABA co-release from SNc^{DA} axons requires Gat1-mediated GABA uptake

(A) Confocal images of SNc in Gat1 cKO^{DA} mice expressing Cre-dependent HA-tagged Gat1 (left) and Gat1(R69K) (right) immunolabeled for TH (green), HA (red), and DAPI (blue). Inset: detailed view (scale, 50 μm).

(B–F) oIPSCs recorded from SPNs (V_h = 0 mV) upon stimulation of SNc^{DA} axons (blue bar) in Gat1 cKO^{DA} mice (B) exogenously expressing Gat1 (C), Gat1(R69K) (D), Gad67 (E), or Aldh1a1 (F).

(G) Fluorescence *in situ* hybridization for Gad67 (red) and TH (green) in Gat1 cKO^{DA} mice with (right) or without (left) Gad67 in DA neurons. Inset: detail (scale, 50 μm).

(H) oIPSC amplitude in SPNs of Gat1 cKO^{DA} mice virally expressing ChR2 in SNc^{DA} neurons (n = 22, p = 1 × 10^{-15}), or ChR2 + Gat1 (n = 14; p = 0.07), ChR2 + Gat1(R69K) (n = 18; p = 1 × 10^{-15}), ChR2 + Gad67 (n = 13; p = 0.018), or ChR2 + Aldh1a1 (n = 17; p = 2 × 10^{-15}) normalized to control. All p values versus control, Mann-Whitney. nd, not detected. Individual values shown along with population mean ± SEM.

(I) Same as (H) for latency (Gat1^{DA}: p = 0.32; Gad67^{DA}: p = 0.0007 versus control, Mann-Whitney).

(J) Same as (I) for rise time (Gat1^{DA}: p = 0.18; Gad67^{DA}: p = 0.39 versus control, Mann-Whitney).

Author Manuscript Author Manuscript Author Manuscript Author Manuscript

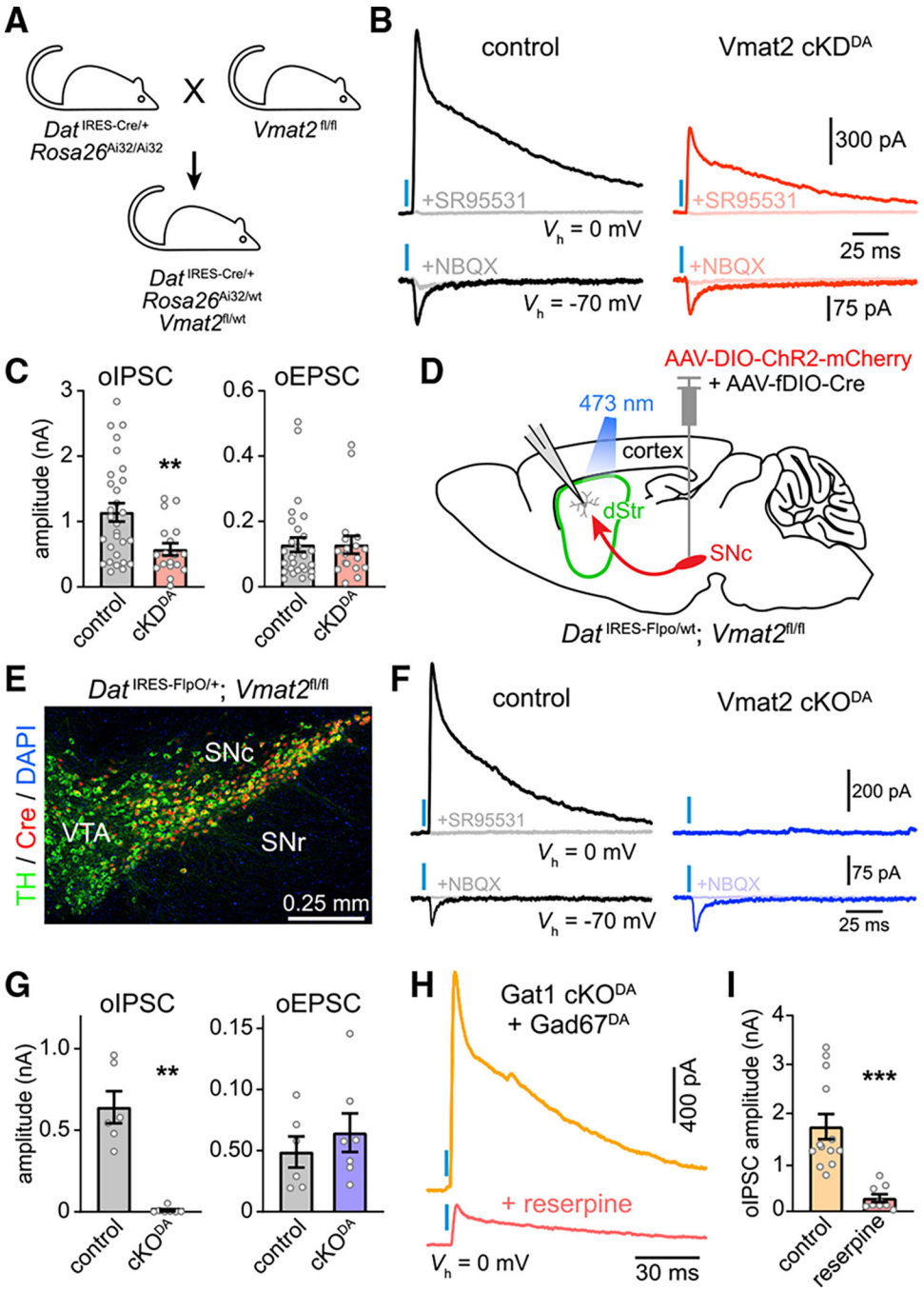

Figure 4. Vmat2 is required for vesicular transport of GABA

(A) Strategy to generate mice in which the expression of ChR2 and Vmat2 in DA neurons is controlled genetically. cKD^{DA} mice have one allele of *Vmat2* conditionally deleted.

(B) Example oIPSCs (top) and oEPSCs (bottom) recorded from SPNs at 0 and −70 mV, respectively, in *Dat*$^{IRES\text{-}Cre/+}$;*Rosa26*$^{Ai32/-}$;*Vmat2*$^{+/+}$ (control; black) and in *Dat*$^{IRES\text{-}Cre/+}$: *Rosa26*$^{Ai32/-}$; *Vmat2*$^{fl/+}$ (Vmat2 cKD^{DA}; red) mice before and after bath application of SR95531 (10 μM) or NBQX (10 μM).

Author Manuscript Author Manuscript Author Manuscript Author Manuscript

(C) Mean amplitude of oIPSCs (left) and oEPSCs (right) recorded from SPNs in control (n = 29) Vmat2 cKD^{DA} (n = 18) mice (p = 0.008, Mann-Whitney). Individual values shown along with population mean ± SEM.

(D) Strategy to conditionally knock out Vmat2 from SNc^{DA} neurons unilaterally in the adult nervous system.

(E) Confocal image of SNc in a *Dat*$^{IRES\text{-}Flpo/+}$; *Vmat2*$^{fl/fl}$ mouse transduced with AAVs encoding Flp-dependent Cre and immunolabeled for TH (green) and Cre (red) showing specific expression of Cre in SNc^{DA} neurons.

(F) Example oIPSCs (top) and oEPSCs (bottom) recorded from SPNs in *Dat*$^{IRES\text{-}Flpo/+}$; *Vmat2*$^{+/+}$ (black) and Vmat2 cKO^{DA} (purple) mice before and after application of SR95531 (10 μM) or NBQX (10 μM).

(G) Same as (C) for control (n = 6) and Vmat2 cKO^{DA} (n = 7) SPNs (oIPSCs: p = 0.0012; oEPSCs: p = 0.53, Mann-Whitney).

(H) oIPSCs recorded from SPNs upon stimulation of Gad67-expressing SNc^{DA} axons (blue bar) in Gat1 cKO^{DA} mice with (red) or without (yellow) reserpine.

(I) Amplitude of oIPSCs in Gat1 cKO^{DA} mice expressing Gad67 in SNc^{DA} neurons without (n = 13) or with reserpine (n = 9; p = 4.02×10^{-6}, Mann-Whitney). Individual values shown along with population mean ± SEM.

Author Manuscript Author Manuscript Author Manuscript Author Manuscript

KEY RESOURCES TABLE

REAGENT or RESOURCE	SOURCE	IDENTIFIER
Antibodies		
Rabbit policlonal anti-Tyrosine Hydroxylase	Millipore	Cat#: AB152; RRID:AB_390204
Mouse monoclonal anti-HA	Abcam	Cat#: ab18181; RRID:AB_444303
Goat ploYclonal anti-Aldh1a1	R&D Systems	Cat#: AF5869; RRID:AB_2044597
Rabbit monoclonal anti-Gat1	Cell Signaling	Cat#: 37342; RRID: AB_2905573
Guinea pig polyclonal anti-Cre-recombinase	Synaptic Systems	Cat#: 257 004; RRID: AB_2782969
Goat anti-mouse IgG Alexa Fluor 488	Thermo Fisher Scientific	Cat#: A11029; RRID:AB_2534088
Goat anti-mouse IgG Alexa Fluor 568	Thermo Fisher Scientific	Cat#: A11004; RRID:AB_2534072
Goat anti-rabbit IgG Alexa Fluor 488	Thermo Fisher Scientific	Cat#: A11034; RRID:AB_2576217
Goat anti-rabbit IgG Alexa Fluor 568	Thermo Fisher Scientific	Cat#: A11036; RRID:AB_10563566
Donkey anti-goat IgG Alexa Fluor 568	Thermo Fisher Scientific	Cat#: A11057; RRID:AB_2534104
Donkey anti-rabbit IgG Alexa Fluor 488	Thermo Fisher Scientific	Cat#: A21206; RRID:AB_2535792
Goat anti-guinea pig IgG Alexa Fluor 568	Abcam	Cat#: ab175714; RRID:AB_2864763
GAT1-Flox14F: TGTGCTGTCCTTCTGGCTGAACATCTACT	This manuscript	N/A
GAT1-Flox18F: TGGAGATAGTCGTTCAGGACAAGCCTACC	This manuscript	N/A
GAT1-Flox15R: AGCATGGCTGGTCAGGGAAGACACTATAG	This manuscript	N/A
Lab ID: GAT1-FloxF: TTCCTGAGTCCCAACATGCCTCG	This manuscript	N/A
GAT1-FloxR: AGTGACAGTGGTGAGTCCATGCAGC	This manuscript	N/A
Bacterial and virus strains		
pAAV-EF1a-double fioxed-hChR2(H134R)-mCherry-WPRE-HGHpA	Addgene	Cat#: 20297-AAV8; RRID:Addgene_20297
pAAV-hSyn-DA2m	Sun et al., 2020	Kindly provided by Dr. Yulong Li
pAAV-EF1a-fDIO-Cre	Addgene	Cat#: 121675-AAV8; RRID:Addgene_121675
pAAV-EF1a-double floxed-Aldh1a1-HA	This manuscript	Cat#: 184633; RRID:Addgene_184633
pAAV-EF1a-double floxed-Gat1-HA	This manuscript	Cat#: 184635; RRID:Addgene_184635
pAAV-EF1a-double floxed-Gat1(R69K)-HA	This manuscript	Cat#: 184636; RRID:Addgene_184631
pAAV-EF1a-double floxed-Gad65	This manuscript	Cat#: 184636; RRID:Addgene_184631
pAAV-EF1a-double floxed-Gad67	This manuscript	Cat#: 184632; RRID:Addgene_184632
Chemicals, peptides, and recombinant proteins		
SR95531	Tocris	Cat#: 1262; CAS#: 104104-50-9
CGP55845 hydrochloride	Tocris	Cat#: 1248; CAS#: 149184-22-5
NBQX disodium salt	Tocris	Cat#: 1044; CAS#: 479347-86-9
R-CPP	Tocris	Cat#: 0247; CAS#: 126453-07-4
Reserpine	Tocris	Cat#: 2742; CAS#: 50-55-5
Critical commercial assays		
Mm-Slc6a1-O1	Advanced Cell Diagnostics	Cat#: 1086931-C3

Author Manuscript Author Manuscript Author Manuscript Author Manuscript

REAGENT or RESOURCE	SOURCE	IDENTIFIER
Mm-Gad1	Advanced Cell Diagnostics	Cat#: 400951-C3
Mm-Gad2	Advanced Cell Diagnostics	Cat#: 439371-C2
Mm-Slc6a3	Advanced Cell Diagnostics	Cat#: 31544-C2
Mm-Th	Advanced Cell Diagnostics	Cat#: 317621
Protease IV	Advanced Cell Diagnostics	Cat#: 322340
Fluorescent Multiplex Detection Reagents: AMP 1, AMP2, AMP 3, AMP 4, DAPI	Advanced Cell Diagnostics	Cat#: 320851
Deposited data		
Data for figures	This manuscript	https://github.com/TritschLab/Melani-Tritsch-2022
Experimental models: Organisms/strains		
B6.C-Tg(CMV-cre)1Cgn/J	Jackson Laboratory (Schwenk et al., 1995)	Strain #: 006054; RRID:IMSR_JAX:006054
B6.SJL-*Slc6a3*$^{tm1.1(cre)Bkmn}$/J	Jackson Laboratory (Bäckman et al., 2006)	Strain #: 006660; RRID:IMSR_JAX:006660
B6.Cg-*Gt(ROSA)26Sor*$^{tm32(CAG-COP4*H134R/EYFP)Hze}$/J	Jackson Laboratory (Madisen et al., 2012)	Strain # 024109; RRID:IMSR_JAX:024109
B6N(Cg)-*Slc6a3*$^{tm1.1(flpo)Fuyu}$/J	Jackson Laboratory	Strain # 033673; RRID:IMSR_JAX:033673
B6.129-*Aldh1a1*^{tm1Gdu}/J	Fan et al., 2003	Kindly provided by Dr. Huaibin Cai
VMAT2$^{fl/fl}$	Isingrini et al., 2016	Kindly provided by Dr. Bruno Giros
Gat1$^{-/-}$	This manuscript	N/A
Gat1^{fl} - B6.Cg-Slc6a1$^{tm1.1Ntrch}$/J	This manuscript	Strain #: 037219
Software and algorithms		
Fiji ImageJ	Schindelin et al., 2012	https://imagej.nih.gov/ij/
Cellpose	Stringer et al., 2021	https://www.cellpose.org/
GraphPad Prism 9.0	GraphPad	RRID:SCR_002798
Custom MATLAB code	Pologruto et al., 2003	RRID:SCR_014307
Igor Pro 6.02A	Wavemetrics	RRID:SCR_000325
OlyVIA 2.8	Olympus	https://www.olympus-lifescience.com/en/discovery/image-sharing-made-easy-meet-olyvia/
ZEN 2.6	Carl Zeiss	https://www.zeiss.com/microscopy/us/products/microscope-software/zen-lite.html
Other		
Fluoromount-G	SouthernBiotech	Cat#: 0100-01
DAPI Fluoromount-G	SouthernBiotech	Cat#: 0100-20
O.C.T compound embedding medium	Fisher Scientific	Cat#: 4585